



Spatial variability of CO₂ uptake in polygonal tundra – large overestimations by the conventional eddy covariance method

Norbert Pirk^{1,2}, Jakob Sievers³, Jordan Mertes^{2,4}, Frans-Jan W. Parmentier^{1,5}, Mikhail Mastepanov^{1,3}, and Torben R. Christensen^{1,3}

¹Department of Physical Geography and Ecosystem Science, Lund University, Sölvegatan 12, 22362 Lund, Sweden

²Geology Department, The University Centre in Svalbard, UNIS, 9171 Longyearbyen, Norway

³Arctic Research Centre, Aarhus University, Denmark

⁴Department of Geological and Mining Engineering and Sciences, Michigan Technological University, 630 Dow Environmental Sciences, 1400 Townsend Drive, Houghton, MI 49931, USA

⁵Department of Soil Quality and Climate Change, Norwegian Institute of Bioeconomy Research (Nibio), Høyskoleveien 7, 1430 Ås, Norway

Correspondence to: Norbert Pirk (norbert.pirk@nateko.lu.se)

Abstract. The large spatial variability in Arctic tundra complicates the representative assessment of CO₂ budgets. Accurate measurements of these heterogeneous landscapes are, however, essential to understand their vulnerability to climate change. We surveyed a polygonal tundra lowland on Svalbard with a UAV, mapping ice-wedge morphology to complement eddy covariance (EC) flux measurements of CO₂. The analysis of spectral distributions showed that conventional EC methods do not accurately capture the turbulent CO₂ exchange with the spatially heterogeneous surface which typically features small flux magnitudes. Non-local (low frequency) flux contributions were especially pronounced during snowmelt and introduced a bias to the annual CO₂ budget of -46 gC m^{-2} in conventional methods. Our improved flux calculations with the ogive optimization method indicated that the site was a sink for CO₂ of -82 gC m^{-2} in 2015 and due to differences in light-use efficiency, wetter areas with low-centered polygons sequestered 47% more CO₂ than drier areas with flat-centered polygons. While Svalbard has experienced a strong increase in mean annual air temperature of more than 2°C in the last few decades, historical aerial photographs from the site indicated stable ice-wedge morphology over the last seven decades. Apparently, warming has thus far not been sufficient to initiate strong ice-wedge degradation, possibly due to the absence of extreme heat episodes in the maritime climate on Svalbard. However, in Arctic regions where ice-wedge degradation has already initiated the associated drying of landscapes, our results suggest a weakening of the CO₂ sink of polygonal tundra.

15 1 Introduction

Carbon-rich Arctic tundra soils are often covered with polygonal ground patterns created by sub-surface ice wedges (*Leffingwell*, 1915; *Mackay*, 1974; *Romanovskii*, 1985; *Minke et al.*, 2007). While ice wedges need centuries or millennia to form through the infiltration and refreezing of meltwater in thermal contraction cracks, they have been reported to degrade rapidly during the last decades with permafrost warming, which significantly alters soil drainage and moisture (*Fortier et al.*, 2007; *Liljedahl et al.*, 2016). Especially in the high Arctic where permafrost warming occurs fastest (*Romanovsky et al.*, 2010), these



hydrological changes can influence the land-atmosphere exchange of greenhouse gases such as carbon dioxide (CO₂), which could affect the long-term carbon sink function of these ecosystems (Schuur *et al.*, 2015; Jorgenson *et al.*, 2015).

CO₂ fluxes in polygonal tundra are characterized by large spatial variability, which complicates their accurate assessment over larger areas (McGuire *et al.*, 2012). On a scale of hectares to km², the micro-meteorological eddy covariance (EC) technique has become widely used to measure the net ecosystem exchange of CO₂ (NEE), because it provides a good compromise between directness of measurement, ecosystem disturbance, and technical reliability. The EC technique estimates NEE integrated over a footprint area upwind based on point measurements of the covariance of vertical wind speed and CO₂ concentration (Aubinet *et al.*, 2012). Careful calculations have been found to provide defensible estimates of the true CO₂ flux, with the main systematic uncertainties stemming from non-steady atmospheric conditions, heterogeneous surfaces and complex terrain (Baldocchi, 2003). Results from different conventionally used software packages for EC calculations have been shown to agree in temperate grasslands and forests (Fratini and Mauder, 2014), but the typically low flux magnitudes in high Arctic environments pose considerable challenges for the correct estimation of EC fluxes (Sievers *et al.*, 2015a). Special care must be taken during the long cold season, when small CO₂ releases can sum up to a significant portion of the total annual carbon budget (Fahnestock *et al.*, 1999; Björkman *et al.*, 2010; Lüers *et al.*, 2014).

Across the Arctic tundra, previous studies have shown differing CO₂ budgets depending on the characteristics of the landscape. EC CO₂ measurements from a well studied high Arctic tundra site in Northeast Greenland indicate a considerable annual carbon sink (−64 gC m^{−2}) in a wet fen (Soegaard and Nordstroem, 1999), while the neighboring dry heath constitutes a weaker sink on average (−21 gC m^{−2}) (Lund *et al.*, 2012). Measurements from Alaskan tussock tundra show that non-growing season releases of CO₂ can also exceed the growing season uptake rendering the ecosystem a small net annual source (+14 gC m^{−2}) (Oechel *et al.*, 2014). A wet tussock grassland in NE Siberia was found to be a moderate annual sink (−38 gC m^{−2}) (Corradi *et al.*, 2005), while wet polygonal tundra in the Lena River Delta was estimated to be a substantial CO₂ sink (−71 gC m^{−2}) (Kutzbach *et al.*, 2007). Some of these studies rely on modeled fluxes to fill large data gaps during wintertime, which increases the uncertainty of the annual sums.

As opposed to other permafrost-underlain regions where soils could become wetter in the future (Natali *et al.*, 2011; Johansson *et al.*, 2013), polygonal tundra is predicted to dry upon permafrost degradation (Liljedahl *et al.*, 2016): the ground above melting ice wedges subsides, which interconnects the polygon troughs and creates an effective drainage network for the wet polygon centers (Fortier *et al.*, 2007). This simultaneous wetting of polygon troughs and drying of polygon centers is a signature that can be detected in time series of historical aerial photographs to provide large-scale evidence of the process (Necsoiu *et al.*, 2013). Liljedahl *et al.* (2016) described such ice-wedge degradation as a widespread Arctic phenomenon, which changed surface drainage patterns in less than one decade. The associated hydrological changes have been linked to significant changes in methane fluxes in Alaskan polygonal tundra (Vaughn *et al.*, 2016), but their larger scale effect on an ecosystem's CO₂ budget is yet to be quantified.

Such an assessment could be improved by high-resolution topographical surveys using unmanned aerial vehicles (UAVs). Apart from the visual picture UAVs provide, the series of photographs from multiple angles allows the reconstruction of the 3D geometry of the surface (Ullman, 1979; Westoby *et al.*, 2012), which can give valuable insights into the drainage patterns.



In the present study, we explore the potential of this technique in combination with EC CO₂ measurements in polygonal tundra on Svalbard to characterize the spatial heterogeneity of the ecosystem. We aim to understand how the spatial heterogeneity and larger-scale disturbances affect EC flux estimates by investigating the spectral composition of the EC signal. We further relate the spatial differences in NEE to the observed historical, and the predicted future evolution of ice-wedge polygons.

5 2 Materials and Methods

2.1 Site description

The field site is located on a river terrace at the bottom of a large, U-shaped, glacial valley called Adventdalen on Spitsbergen, Svalbard, approximately 6 km from a fjord (78°11'N, 15°55'E). Wind directions are generally oriented along the valley, with dominating easterlies in wintertime, and an approximately even distribution of easterlies and westerlies in summertime. The mean annual air temperature at the closest weather station (Svalbard airport, approximately 10 km away) was -6.7°C between 1961 and 1990 (Førland *et al.*, 2012), which has increased to -3.75°C in the period between 2000 and 2011 (Christiansen *et al.*, 2013). The total annual precipitation is about 190 mm, of which about half falls as snow (Førland *et al.*, 2012). The landscape setting in combination with these climatic conditions created a continuous permafrost fen, in which the ground is patterned by low-centered ice-wedge polygons (Christiansen, 2005; Harris *et al.*, 2009). The vegetation at the Adventdalen site features *Salix polaris* in drier areas, *Eriophorum scheuchzeri* and *Carex subspathacea* in wetter locations, and moss species in usually inundated spots.

2.2 Measurement setup

The EC setup consisted of a top-mounted ultra-sonic anemometer (USA-1, Metek GmbH, Germany) and an infra-red gas analyzer (Li-7200, Li-Cor Inc., USA), both of which were sampling and recording data at a rate of 10 Hz. The measurement height was 2.8 m above ground level. From there the gas was pumped to the Li-7200 at a flow rate of 15 L min⁻¹ via a 1 m long, insulated intake tube supplied by the manufacturer. We mainly focused on data collected between September 2014 and December 2015, when data quality and coverage was highest. CO₂ concentrations collected in 2013 were only recorded as wet molar densities and without the cell pressure necessary to convert them to dry mixing ratios. We therefore consider 2013's fluxes less certain and only use them as supplementary support for our findings.

Ancillary meteorological measurements (e.g. solar radiation, snow and soil temperatures) were collected on and around the same tower, sampled every 10 sec and averaged to 30 min values. Due to the relatively remote location without line power, the system was supplied by lead-acid batteries, which were charged by a wind generator (350 W peak output) and solar panels (275 W peak output), as well as a fuel cell in summertime (90 W).

Complementary to the EC setup, we measured NEE in the EC footprint with a set of five transparent, automatically operated, flux chambers using the closed chamber technique. These chambers were connected to a gas analyzer (SBA-4, PP Systems, UK), which measured CO₂ concentrations at a rate of 0.625 Hz. Flux estimates were derived from exponential least-squares



regression of the 5 min closure time of the concentration time series (details of this measurement system and flux estimation procedure are provided in *Pirk et al.* (2016b) and references therein).

To assess differences in the active layer depth, thaw depths were probed at the centers of 30 polygons in the EC footprint at the end of August 2016.

5 2.3 Data processing

EC flux estimates were derived using the recently proposed ogive optimization method (version 1.0.5, toolbox publicly available through the Mathworks file exchange) (*Sievers et al.*, 2015b). In this context, ogives are cumulative co-spectra of vertical wind speed (w) and CO_2 concentration (denoted $\text{Og}(w, \text{CO}_2)$), i.e. a spectral decomposition of the EC flux estimate. The method optimizes a spectral distribution model (*Desjardins et al.*, 1989; *Lee et al.*, 2006; *Foken et al.*, 2006) to a density map of 14 000
 10 ogives obtained by varying the dataset length and de-trending interval. The key to this method is the assumption of a dynamic spectral gap between often overlapping spectral flux contributions (*Sievers et al.*, 2015b). This approach effectively separates the turbulent flux from contributions of larger-scale motions (mesoscale atmospheric movements), which can give non-local flux contributions at low frequencies (*Aubinet et al.*, 2012; *Sievers et al.*, 2015b).

To further investigate the effect of low frequency contributions we compared ogive optimization to the widely used EddyPro
 15 software package (Li-Cor Inc., version 6.1.0), following the conventional assumption about the presence of a fixed spectral gap corresponding to the 30 min flux averaging interval. We used simple linear de-trending, and applied spectral corrections according to *Moncrieff et al.* (1997, 2004) (EddyPro default).

Both EddyPro and ogive optimization perform basic quality control and pre-processing of the 10 Hz raw data following *Vickers and Mahrt* (1997) (e.g. gap detection, spike removal, signal alignment, anemometer tilt correction). Unacceptable
 20 raw data were not processed further. To ensure sufficient turbulent mixing near the surface, we also filtered out data points with a friction velocity smaller than 0.1 m sec^{-1} for both methods. Following *Foken and Wichura* (1996), EddyPro fluxes were additionally filtered for non-steady wind conditions (discarding fluxes with quality flag 2). Calculated ogive optimization fluxes, on the other hand, were only discarded if the modeled ogive spectral distribution could not describe the data sufficiently well. These filters, in addition to down-time caused by technical problems, led to an overall data coverage with valid fluxes of
 25 45% in 2015 for the ogive optimization and 35% with EddyPro. A large number of these flux calculations have been visually inspected to ensure that the methods performed as expected. In this analysis, we noticed that the automatically determined time lags between w and CO_2 concentration varied unrealistically, which introduced noise to the fluxes—especially at low magnitudes. We therefore used a constant value of 0.3 sec (i.e. the typically expected time lag given our setup) for the flux calculation with both methods.

30 Subsequently, the calculated NEE was used to determine the ecosystem's light response characteristics during the snow-free period (beginning of June until end of September). One way to parameterize the relationship between NEE and incoming photosynthetically active radiation (PAR) is the Misterlich function,

$$\text{NEE} = -(F_{\text{csat}} + R_d) \left(1 - \exp \left(- \frac{\alpha \text{PAR}}{F_{\text{csat}} + R_d} \right) \right) + R_d, \quad (1)$$



where the three parameters F_{csat} , R_{d} , and α correspond to the flux at light saturation, dark respiration, and light-use efficiency, respectively (e.g., *Falge et al.*, 2001). Such light response curves can yield further insights to the underlying drivers of NEE. These parameters were derived from least-squares regressions of measured NEE and PAR (derived from short wave incoming radiation) in a rolling time window of 10 days, which was successively increased by 1 day if less than 100 valid NEE-PAR
5 measurements were available (following *Lund et al.* (2012)).

For cumulative flux calculations and annual sums we employed the gap-filling algorithm proposed by *Reichstein et al.* (2005), which operates on the basis of mean diurnal variations of temperature, incoming short wave radiation, and vapor pressure deficit as drivers for NEE. As some of the gaps in our NEE measurements were caused by power outages (when the entire measurement system shut down), the ancillary data for gap-filling were taken from the New Adventdalen Weather
10 Station (run by the University Centre in Svalbard) with a distance of about 2.5 km from our site (typical meteorological data correlations $r > 0.9$). This procedure yielded the best gap-filling quality (class A) in 96% of the flux estimates that had to be gap-filled in 2015. Still, gaps in NEE measurements can be assumed to dominate the total random error of the annual sums (*Aurela et al.*, 2002). To quantify this uncertainty, we tested the sensitivity of the annual sums to artificially added gaps in the NEE time series. Since the uncertainty introduced by a gap depends on its length and time of year, we repeated the gap-filling
15 on 300 different time series obtained by adding single gaps with a length between 1 and 23 days (i.e. 2 days longer than our longest gap) which were equally distributed over the year (starting every 15 days). The resulting distribution of annual sums was used to assess the result's random error.

The EC footprint estimation was performed according to *Kljun et al.* (2015), using a fixed zero-plane displacement of 10 cm, and a roughness length of 1 cm. Wind and turbulence parameters were derived from 30 min intervals, while the additionally
20 needed boundary layer height was taken from the closest point of the Era-Interim meteorological reanalysis (*Dee et al.*, 2011).

2.4 Topographical survey

We conducted a topographical survey of the Adventdalen ice-wedge site employing photogrammetry of aerial photographs to produce a visual map and digital elevation model. To this end, 135 photographs were taken with a camera (GoPro Hero3+ Black Edition) from a UAV (DJI Flamewheel 550) at a height of 60 m a.g.l. in June 2015. This survey covered an area of
25 about 0.1 km² at a ground resolution of about 3.2 cm pixel⁻¹. 22 ground control points were collected with a differential GPS (Leica GPS1200 SmartRover) to ortho-rectify the images and estimate the uncertainty of the resulting elevation model (see Fig. S5 in the supporting information for details). GPS data were post-processed and differentially corrected using data from the local Longyearbyen GNSS satellite basestation (LYRS), which is freely available from the Norwegian Mapping Authority. The photogrammetric processing was performed using Agisoft PhotoScan (Agisoft LLC, St. Petersburg, Russia), which implements
30 the structure-from-motion technique to reconstruct the 3D geometry of the ground surface from the sequence of photographs taken from multiple viewpoints (*Ullman*, 1979; *Snively et al.*, 2008; *Westoby et al.*, 2012; *Lucieer et al.*, 2013).

To assess the evolution of the morphology of the ice-wedge site, we compared our map from 2015 to historical aerial photographs taken 1948, 1961 and 1990, which were geo-referenced with 2015's map as a reference. Reliably quantifying the



changes between these images was complicated by different shadows and overall soil moisture when the images were taken, so we only performed a qualitative change detection by visual comparison.

3 Results

Figure 1 shows the results of the topographical survey and the EC footprint for June 2015. As the wind direction typically aligns with the valley's direction, there are two clearly distinct footprint areas in the NW and ESE. The high resolution of this elevation map resolves small elevation differences of only a few decimeters, which can be seen to affect surface inundation and soil wetness. Both footprints have overall surface slopes toward the edge of the river terrace in the north (approximately 0.75% slope), but their drainage patterns appear to be separated creating a wetter sub-catchment in the NW than in the ESE. Low-centered polygons dominate the site, but the NW features more distinctly wet polygon centers. The thaw depth at the centers of the polygons around the EC tower was on average 66 cm (standard deviation=9 cm) by the end of August. Based on the polygons in the 50% EC footprint, the drier ESE fetch area had on average 10 cm larger thaw depths than the wetter NW, but due to the large variations this difference is not statistically significant.

The shown surface heterogeneity is likely to lead to spatial variations of NEE in the EC footprint. To assess this effect and mesoscale disturbances, we investigated the spectral composition of the EC signal by looking at the ogives of vertical wind speed and CO₂ concentration. Particularly around the time of snowmelt, we often found a mismatch between lower and higher frequencies indicating different local and non-local flux contributions. Figure 2a shows an example from this period comparing the ogives of conventional flux calculations produced by EddyPro and ogive optimization flux estimation based on the ogive density map. While all frequencies contribute fully to the conventional flux estimation, frequencies can obtain less weight in the ogive optimization method if they cannot be described by the ogive spectral distribution model. In the given example, this conceptual difference of the methods means that ogive optimization indicated a CO₂ release, while EddyPro indicated uptake. Spectral corrections had a comparably small effect. During this period in May and June the surface was a mix of patches of snow-free soil, remaining snow, and meltwater ponds (when a net CO₂ uptake can be considered unlikely, see Fig. 2b). The low frequency contributions also depend on larger-scale atmospheric movements, while the local turbulent flux is represented better in the mid-to-high frequency range. Such frequency mismatches were frequently observed in our data and their effect was relatively largest for the small non-growing season fluxes (see Fig. S1 in the supporting information for additional ogive examples and Fig. S3a for a flux comparison). The shifts between release and uptake of CO₂ typically occurred at frequencies below 10⁻¹ Hz, corresponding to recorded eddies with a diameter of typically more than 30 m at the given wind speed. During the growing season, fluxes from both methods typically agreed. Photos of the site in different seasons are given in Fig. S6 in the supporting information.

Due to its better performance, we used NEE fluxes calculated by the ogive optimization method for the ecosystem characterization. Figure 3 shows the gap-filled NEE fluxes of 2015 as fingerprint plots, as well as cumulative sums, which were also calculated after separately gap-filling the measurements of the two distinct footprints (NW and ESE). These results indicate that the growing season in 2015 started on 14 June and ended 28 August (defined as first until last day of net CO₂ uptake). Re-

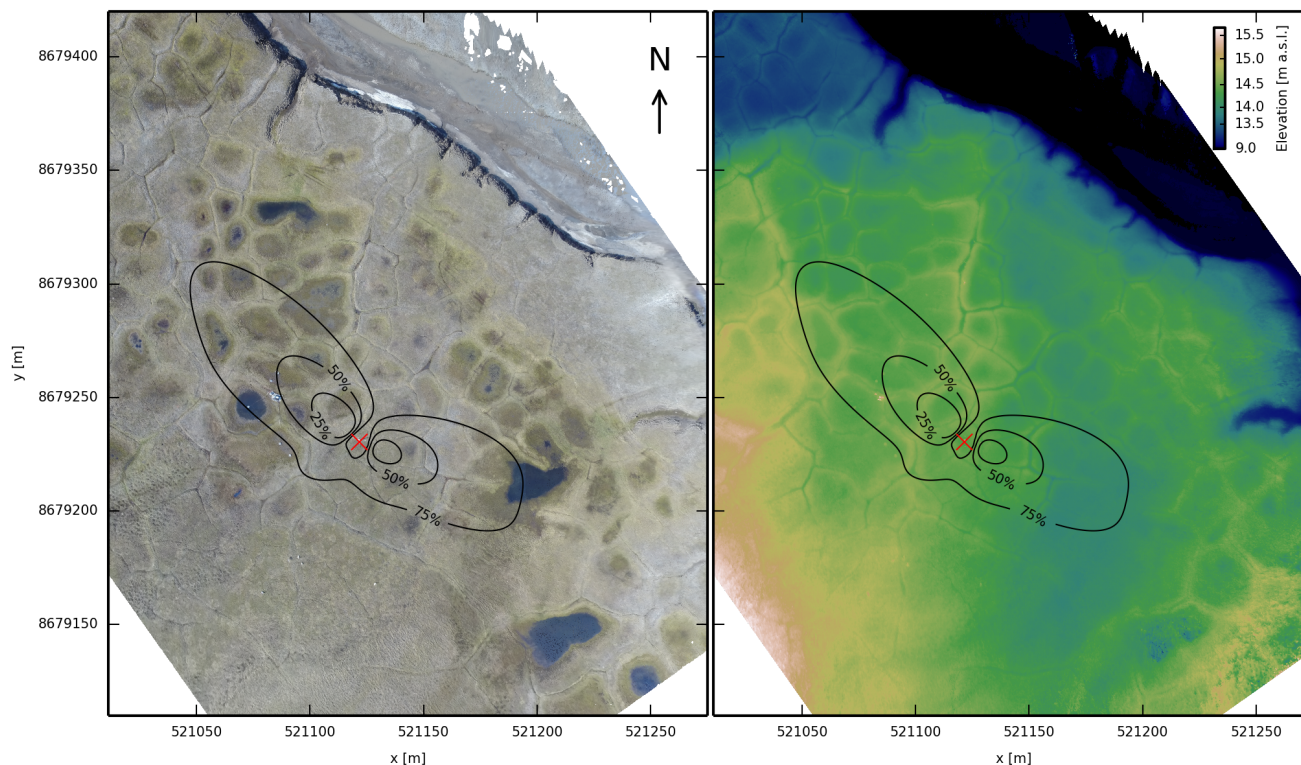


Figure 1. Map of the site in Adventdalen (coordinates in UTM zone 33X). The red cross marks the EC tower, around which the contour lines indicate the area's relative contribution to the EC signal (footprints) averaged over June 2015. Six automatic flux chambers are located in the NW footprint (bright dots). Left: Ortho-rectified aerial photograph from end of June 2015. Right: Corresponding surface elevation with an estimated vertical uncertainty of 0.2 m.

sults from EddyPro indicated the same date for the end of the growing season, while its start was suggested already one month before snowmelt. The fingerprint plot (Fig. 3a) shows that there can even be CO₂ uptake at midnight during the polar day in the summer. While the drier ESE yielded an annual carbon balance of -62 gC m^{-2} , the wetter NW yielded -91 gC m^{-2} . The annual balance of the combined footprint was -82 gC m^{-2} in 2015. The corresponding value based on EddyPro flux calculations was -128 gC m^{-2} , which we consider biased by the above-mentioned low frequency contributions. The relatively narrow probability distributions of the annual sums (based on gap-filling uncertainties) demonstrate the significance of the differences between the NW and ESE footprints, as well as between the ogive optimization and EddyPro methods. Relatively large annual sinks are supported by our automatic closed chamber measurements in the NW footprint which show good agreement and correlation ($0.75 < r < 0.88$, $p < 10^{-12}$) with the EC fluxes (see Fig. S3b in the supporting information). In 2013, EddyPro calculations yielded a smaller total annual CO₂ balance of -79 gC m^{-2} (see Fig. S2d in the supporting information), whereas

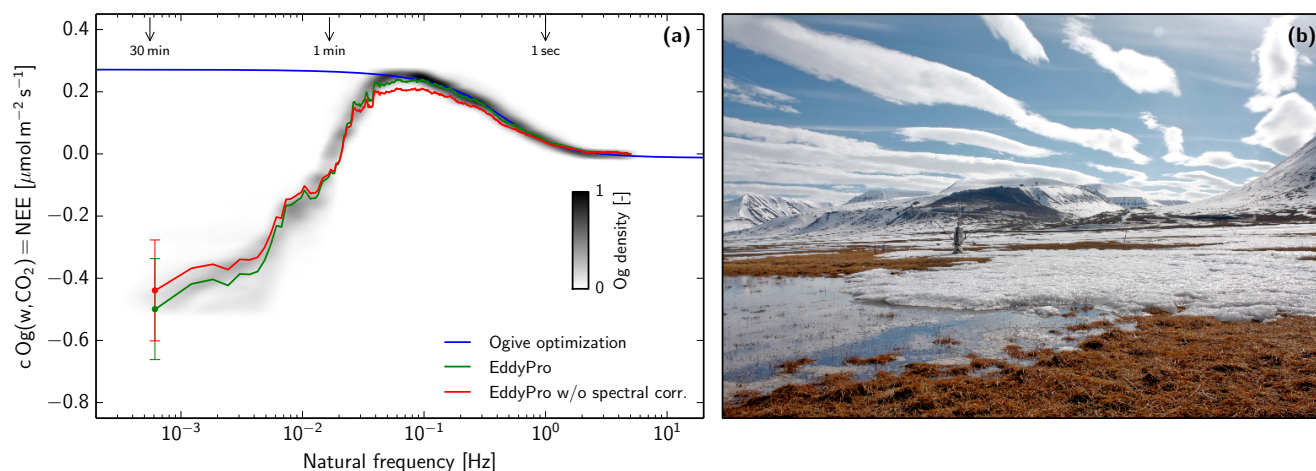


Figure 2. Example of the CO₂ flux estimation during snowmelt. a: Ogives on 31 May 2015, 15:00 LT, showing a mismatch between low and high frequencies. While ogive optimization estimates a net CO₂ release, EddyPro (with and without spectral corrections after *Moncrieff et al. (1997, 2004)*) indicates an uptake. Average horizontal wind speed was 5.2 m sec⁻¹ from NW (313°), air temperature 4.5°C, quality flag 0. Arrows on the top indicate the corresponding time scales. b: Photo of the environment around the flux tower at that time.

ogive optimization fluxes could not be calculated from these raw CO₂ measurements since they were wet rather than dry molar densities.

Much of the spatial differences in the annual CO₂ budget stem from the growing season, when NEE is strongly affected by PAR. Figure 4 shows examples of the derived light response curves, as well as the evolution of the associated dark respiration and light-use efficiency throughout the growing season. Both dark respiration and light-use efficiency were typically higher in the wetter footprint (NW) than in the drier (ESE), consistent with the larger annual uptake in the NW than the ESE. At the beginning and end of the growing season, the determination of the flux at light saturation (F_{csat}) was associated with relatively large uncertainties, because NEE and PAR varied relatively little. During the peak growing season F_{csat} was about 6.6 $\mu\text{mol m}^{-2} \text{s}^{-1}$ for both footprints. The sum of F_{csat} and R_d can be used to estimate the gross primary productivity at light saturation, which was found to be $-11.0 \mu\text{mol m}^{-2} \text{s}^{-1}$ in the NW and $-8.3 \mu\text{mol m}^{-2} \text{s}^{-1}$ in the ESE. During snow covered conditions outside the growing season, our measurements indicated an overall decreasing trend of the small CO₂ releases throughout winter, which was modulated by increases during strong winds (see Fig. S4 in the supporting information). Soil temperature, on the other hand, had no strong effect on the wintertime CO₂ release despite a large variation of more than 25°C (cf. Fig. S4c).

Figure 5 shows a time series of ortho-rectified aerial photographs covering the same area as Fig. 1. Despite the differences in image quality, shadows and overall soil moisture on the days these images were taken, the time series still gives an impression about the development of the polygon morphology. All images show the same, low-centered polygons, whose centers were about equally inundated (except in 1990 when the area was drier in general). There was no clear lateral expansion or degradation

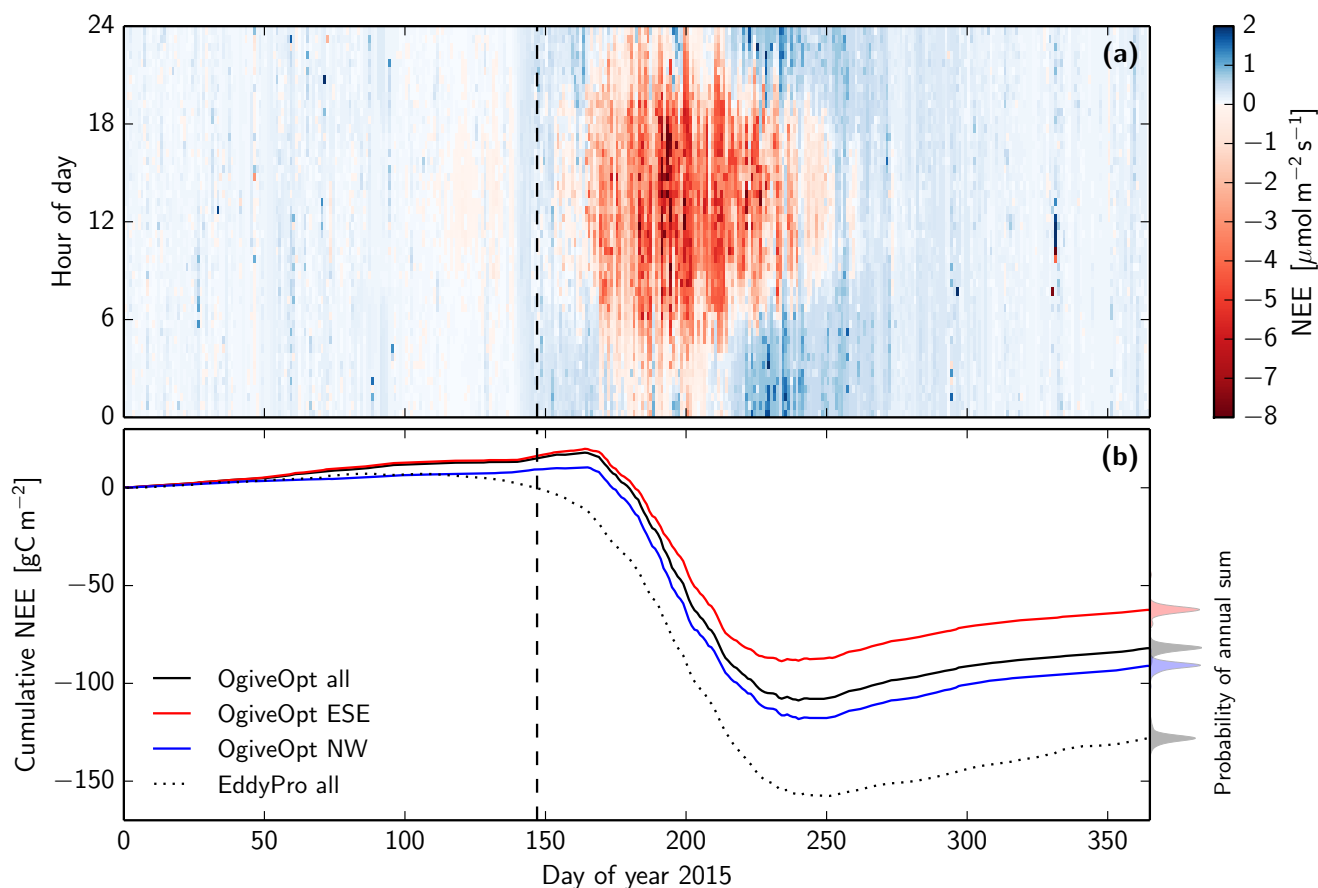


Figure 3. Gap-filled NEE fluxes for 2015. a: Fingerprint plot of ogive optimization results. b: Corresponding cumulative sums based on all valid measurements (black), and separately gap-filled for the two footprints (colored). The probability distributions shown on the right indicate the estimated uncertainty of the annual sum due to data gaps and gap-filling. The dashed line marks the time during snowmelt when daily average albedo dropped below 0.3 (27 May 2015).

of the polygon troughs. Neither the ponds nor the troughs became more interconnected or wet in general, so there are no clear signs of differential ground subsidence at this site. Also other areas with ice-wedge polygons in Adventdalen indicated the same, stable morphology during the last seven decades (see Fig. S7 in the supporting information). Between 1990 and 2015, some erosion on the edge of the river terrace occurred. The exact speed of this edge erosion is hard to quantify due to the shadows in this area, but it did not exceed 3 m over these 15 years. The photograph from 1990 was taken in the near infra-red range and is shown in false colors. Vegetation, bare soil, and open water reflect near infra-red light differently, so this image clearly depicts these surfaces. The strong red tones in the NW footprint correspond to the relatively high vegetation density in this area, which was also seen in Fig. 1. The river in the NE appears in a blue tone, while darker spots in the SW corner of the image correspond to an area with bare soil brought to the surface by cryoturbation.

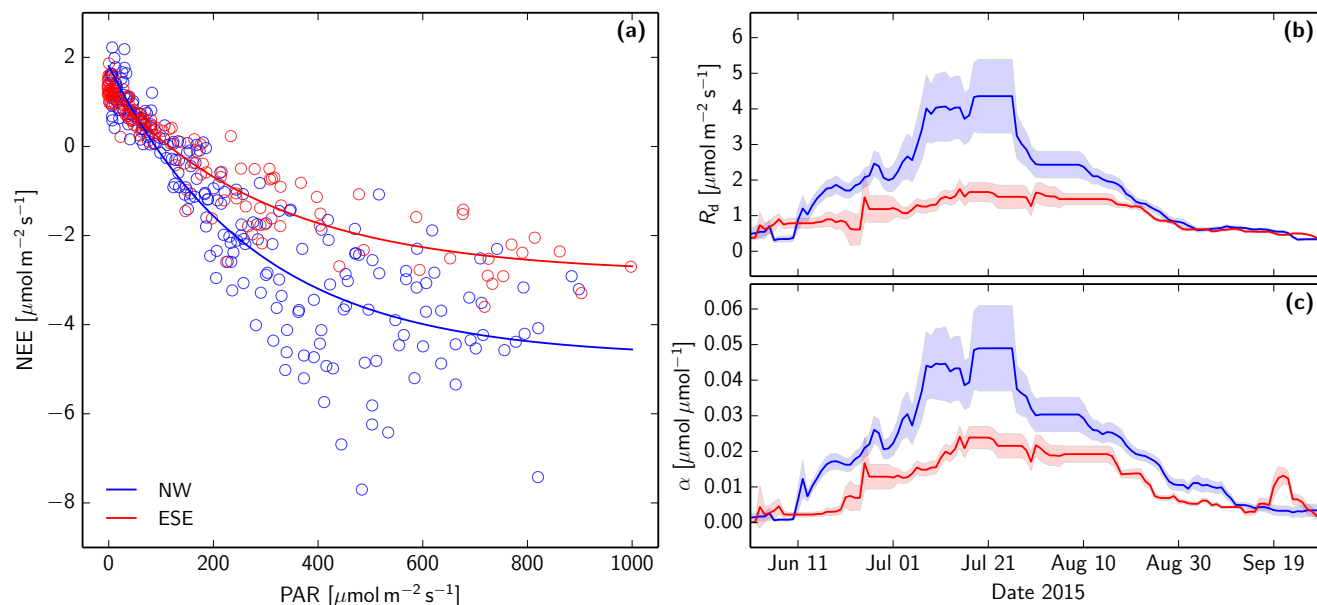


Figure 4. Growing season NEE light response curves based on the ogive optimization method. a: Examples from the time window around 18 August 2015 from the two distinct footprints. b: Time series of dark respiration parameters. c: Corresponding graph for light-use efficiency. Shaded bands indicate the statistical standard error of the parameters.

4 Discussion

Our measurements demonstrate the high sensitivity of carbon cycling to small topographic differences in permafrost-underlain Arctic tundra. Ice-rich permafrost is particularly vulnerable to warming, with large increases in permafrost degradation documented in the last two decades (Jorgenson *et al.*, 2006; Osterkamp *et al.*, 2009; Grosse *et al.*, 2011). Liljedahl *et al.* (2016) observed pan-Arctic permafrost degradation in polygonal tundra which dramatically changed the local drainage patterns and water balance on sub-decadal timescales. Ice-wedge melting and the associated differential ground subsidence is expected to interconnect formerly separated trough networks and thereby increase the drainage of polygon centers (Necsoiu *et al.*, 2013; Jorgenson *et al.*, 2015; Liljedahl *et al.*, 2016). At a later stage this process transforms low-centered polygons into high-centered polygons and leads to the overall drying of the entire landscape. In such cases, the space-for-time substitution of our two distinct footprint areas in Adventdalen would suggest a corresponding lessening of CO_2 sinks in degrading polygonal tundra.

However, our comparison of aerial photographs taken between 1948 and 2015 shows that there is no dramatic ice-wedge degradation at our site on Svalbard. Nearby areas with polygonal tundra in Adventdalen have also been stable during the last seven decades, despite the measured increase of 2.95°C in mean annual air temperatures between the periods 1961–1990 and 2000–2011 (Førland *et al.*, 2012; Christiansen *et al.*, 2013; Nordli *et al.*, 2014). The maritime climate on Svalbard prevents episodes with extremely high summer temperature, which have been hypothesized to trigger ice-wedge degradation (Jorgenson *et al.*, 2006; Liljedahl *et al.*, 2016). It appears that the gradual climate warming alone has so far not been sufficient to initiate

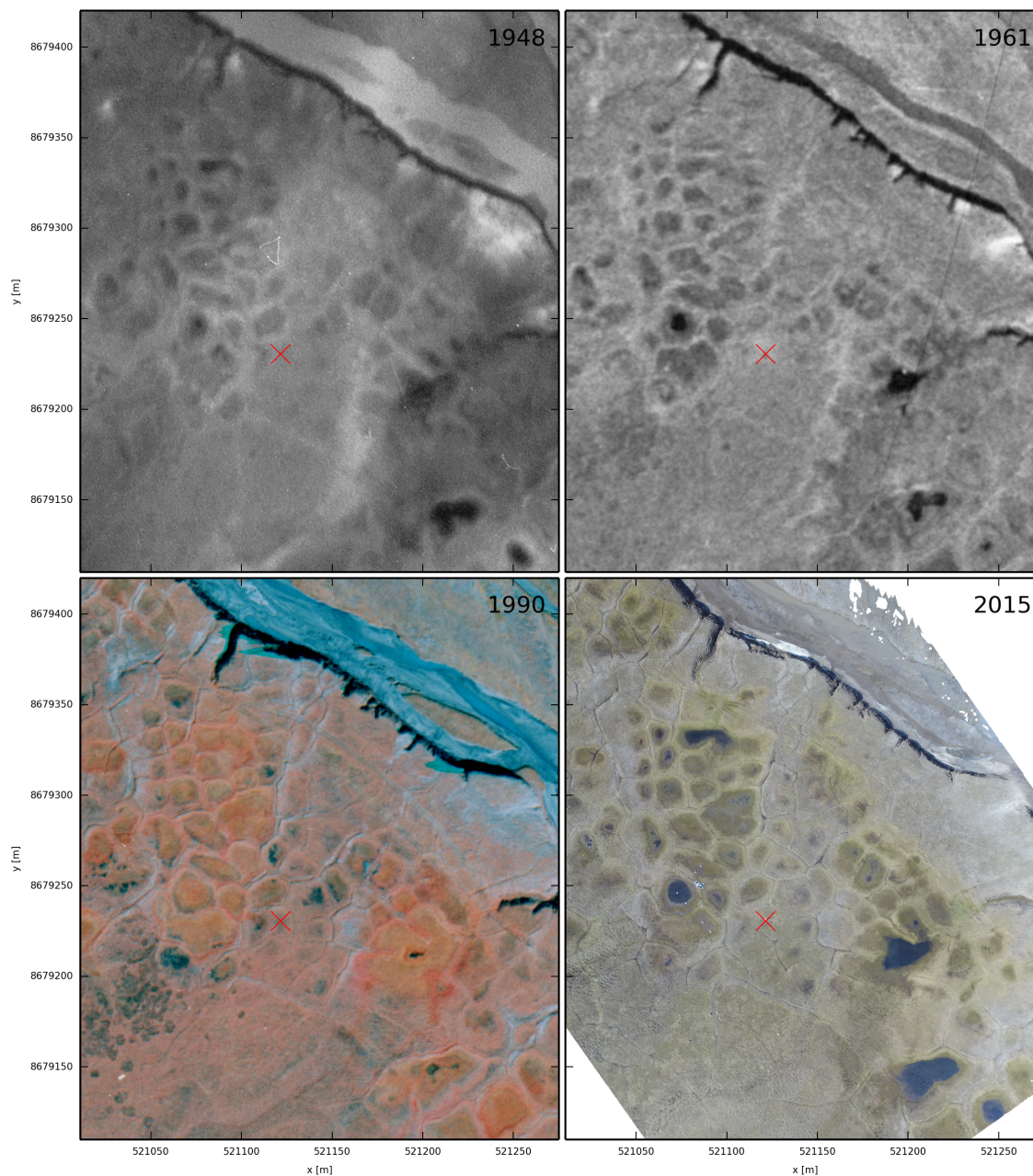


Figure 5. Time series of images of the Adventdalen site showing little signs of differential ground subsidence, which would indicate ice-wedge degradation. The image from 2015 is the same as shown in Fig. 1, while historical photographs were provided by the Norwegian Polar Institute (reference numbers S48-5181, S61-3301 and S90-5273). The images from 1948 and 1961 were taken on panchromatic films, and the image from 1990 is a near infra-red (false color) photography. The red cross marks the EC tower.



strong ice-wedge degradation in Adventdalen. Another reason for the apparent stability of the ice wedges at our site could be the relatively small surface slope of typically less than 1%, which hinders the development of an effective drainage system of degraded troughs. Generally speaking, ice-wedge stabilization can also be caused by negative feedbacks such as increased plant growth in degraded troughs which cools the soil above the ice wedge (*Jorgenson et al.*, 2015). Despite these mechanisms and observations, the strong temperature increase on Svalbard may eventually lead to the gradual degradation of ice wedges in Adventdalen, which we argue will lessen the CO₂ sink of this ecosystem.

The overall annual CO₂ balance of -82 gC m^{-2} seems surprisingly large, given the high northern location of the site with its typically shallow organic horizon in the soil (5–10 cm). The good agreement of EC and automatic closed chamber measurements, however, confirms the relatively high uptake fluxes in the snow-free period. Also the comparison of the light response curve parameters to other Arctic sites indicates high, but realistic, growing season productivity. *Mbufong et al.* (2014) derived these parameters from 12 Arctic tundra sites during the peak growing season and report R_d between 0.6 and $3.9 \mu\text{mol m}^{-2} \text{ s}^{-1}$, and α between 0.011 and $0.057 \mu\text{mol } \mu\text{mol}^{-1}$. Peak season parameters for the drier footprint (ESE, $R_d \sim 1.7 \mu\text{mol m}^{-2} \text{ s}^{-1}$, $\alpha \sim 0.024 \mu\text{mol } \mu\text{mol}^{-1}$) at the Adventdalen site lie well in the center of this range, while the wetter footprint (NW, $R_d \sim 4.3 \mu\text{mol m}^{-2} \text{ s}^{-1}$, $\alpha \sim 0.049 \mu\text{mol } \mu\text{mol}^{-1}$) lies on the upper end of this reported range. These values, in combination with the relatively large amount of incoming shortwave radiation at 78°N during summertime, explain the large carbon sink in Adventdalen. Especially the wetter areas lose some carbon through methane emissions, but our automatic chamber measurements indicate that these losses are not expected to exceed 6 gC m^{-2} per year (*Pirk et al.*, 2016a). We consider the export of dissolved organic carbon negligible, because the small surface slope and limited conductivity prevents a pronounced lateral water runoff.

The grazing pressure from Svalbard reindeer could represent another type of carbon loss, which has not been quantified in the present study. Moreover, *Wegener and Odasz-Albrigtsen* (1998) observed that plants in Adventdalen balance the consumption by reindeer with increased plant productivity. While such interactions influence the carbon budget of the ecosystem, they do not affect the discrepancy we found between the two EC flux calculation methods.

The drivers of cold season emissions of CO₂ from high Arctic tundra are still understudied, because technical challenges and low flux magnitudes often complicate continuous in-situ flux measurements. Our wintertime flux measurements from Adventdalen were found to decrease slightly throughout winter. Episodic flux increases correlated with wind speed, suggesting a convective mixing of the snowpack gas reservoir as observed in other studies from lower latitudes (*Takagi et al.*, 2005; *Seok et al.*, 2009; *Smagin and Shnyrev*, 2015). The missing relation between soil temperature and measured wintertime CO₂ release could suggest a decoupling of CO₂ production and release caused by the physical blockage of gas diffusion in the soil (*Elberling and Brandt*, 2003) or through potential ice layers in the snowpack (*Pirk et al.*, 2016a). While the majority of wintertime fluxes were positive, some small uptake fluxes have also been observed during the dark, snow covered period. Unlike reports from other sites (*Lüers et al.*, 2014), these fluxes have no significant impact on the annual CO₂ budget of our site. As photosynthesis by plants or snow algae can be excluded during the dark polar night, one might speculate that the apparent uptakes are caused by abiotic mechanisms, such as the convective mixing of CO₂-depleted gas stored in the snowpack or thermo-physical processes related to CO₂ solubility in unfrozen pore water. Yet we found no relationship between uptake situations and changes in snow,



air or soil temperatures, or ambient atmospheric CO₂ concentrations—which could support potential abiotic mechanisms of CO₂ uptake. The magnitude of these fluxes was also so low compared to biotic flux contributions that they cannot markedly change the overall annual CO₂ balance of the ecosystem.

The conceptual definition of turbulent fluxes differs fundamentally between the ogive optimization and conventional methods as implemented in EddyPro. While the ogive optimization assumes a unidirectional flux, which is sometimes better captured in the mid and high frequency range, EddyPro includes all frequencies regardless of their direction. The ogive optimization method appeared better suited for the Adventdalen site than conventional processing schemes. Specifically around the snowmelt period, the ogive optimization estimates appear to capture the local flux signal more realistically than conventional calculations, which indicated an onset of the growing season already before snowmelt. This contradiction was caused by many bi-directional fluxes, i.e. situations with a consistent CO₂ release reflected in high frequencies and CO₂ uptake reflected in the low frequency range of the spectrum (cf. Fig. 2a and Fig. S1). The shift between these contributions occurred at frequencies corresponding to eddies with a diameter of more than 30 m, i.e. exceeding the typical dimension of surface heterogeneity in the footprint area of our site. One might speculate that the systematic occurrences of bi-directional fluxes are due to an atmospheric layering where low and high frequency eddies circle through air masses with different CO₂ concentrations: While the (smaller) high frequency eddies only reflect one air mass, the (larger) low frequency eddies reflect two air masses with different CO₂ concentrations. In the specific environment in Adventdalen, such a layering might be induced by the intrusion of CO₂-depleted air at the surface originating from the surrounding mountains by way of katabatic winds, or sea breeze circulations from the nearby fjord (*Esau and Repina, 2012*). However, similar low frequency shifts were also observed in environments with neither pronounced surface heterogeneity nor nearby water or mountains (*Sievers et al., 2015b*). Across the different sites we see a tendency for low frequency shifts to occur predominantly during conditions with small flux magnitudes, when the normally dominating mid and high frequency contributions can be much smaller than (non-local) low frequency contributions. So perhaps the hypothetical layering of the atmosphere is caused by the repeatedly changing CO₂ flux at the surface in response to diurnal factors such as changes in incoming solar radiation, which give rise to CO₂ concentration waves propagating vertically into the atmosphere. While such hypotheses remain to be investigated in future studies, we show that these (non-local) low frequency contributions lead to a difference in the annual CO₂ budget of -46 gC m^{-2} over the course of one year (cf. Fig. 3b). The ogive optimization method is more applicable to these highly heterogeneous, Arctic environments dominated by small fluxes because it can separate local and non-local flux contributions.

5 Conclusions

The Adventdalen ice-wedge site was a surprisingly strong CO₂ sink in 2015 (-82 gC m^{-2}). Differences in vegetation density and composition lead to a significantly higher light-use efficiency in areas with low-centered ice-wedge polygons compared to flat-centered polygons. While dark respiration in the wetter area was also higher than in the drier area, these releases did not compensate for the higher light-use efficiency in the annual CO₂ balance. In 2015, the drier area sequestered 32% less CO₂ than the wetter area (-62 compared to -91 gC m^{-2}). These results suggest a high sensitivity of CO₂ dynamics to small



topographic differences in Arctic tundra ecosystems. With climate warming, ice wedges are predicted to melt and dry out the landscape. Despite strong increases in mean annual air temperatures of more than 2°C on Svalbard in the last few decades, we see no evidence of ice-wedge degradation compared to historical aerial images. However, further warming may eventually initiate ice-wedge degradation, and our spatial analysis implies a corresponding reduction of the CO₂ sink upon drying. In
5 Arctic polygonal tundra where drying is occurring already, our results therefore suggest a similar weakening of the CO₂ sink function.

6 Data availability

Maps, measurement data and processing scripts are available from the authors upon request (norbert.pirk@nateko.lu.se).

Competing interests. The authors declare that they have no conflict of interest.

10 *Acknowledgements.* The research leading to these results has received funding from the European Community's Seventh Framework Program (FP7) under Grants 238366, 262693 and 282700, and the Nordic Centers of Excellence DEFROST and eSTICC (eScience Tool for Investigating Climate Change in northern high latitudes) funded by Nordforsk (grant 57001). We thank Sarah Strand and Andreas Alexander (UNIS) for their work at the Adventdalen site, and Sebastian Westermann (University of Oslo) for providing computational resources needed for the data processing.



References

- Aubinet, M., T. Vesala, and D. Papale (2012), *Eddy covariance: a practical guide to measurement and data analysis*, Springer Science & Business Media.
- Aurela, M., T. Laurila, and J.-P. Tuovinen (2002), Annual CO₂ balance of a subarctic fen in northern Europe: importance of the wintertime
5 efflux, *Journal of Geophysical Research: Atmospheres*, *107*(D21).
- Baldocchi, D. D. (2003), Assessing the eddy covariance technique for evaluating carbon dioxide exchange rates of ecosystems: past, present and future, *Global Change Biology*, *9*(4), 479–492.
- Björkman, M. P., E. Morgner, E. J. Cooper, B. Elberling, L. Klemetsson, and R. G. Björk (2010), Winter carbon dioxide effluxes from Arctic ecosystems: an overview and comparison of methodologies, *Global Biogeochemical Cycles*, *24*(3).
- 10 Christiansen, H. H. (2005), Thermal regime of ice-wedge cracking in Adventdalen, Svalbard, *Permafrost and Periglacial Processes*, *16*(1), 87–98.
- Christiansen, H. H., O. Humlum, and M. Eckerstorfer (2013), Central Svalbard 2000–2011 meteorological dynamics and periglacial landscape response, *Arctic, Antarctic, and Alpine Research*, *45*(1), 6–18.
- Corradi, C., O. Kolle, K. Walter, S. Zimov, and E.-D. Schulze (2005), Carbon dioxide and methane exchange of a north-east Siberian tussock
15 tundra, *Global Change Biology*, *11*(11), 1910–1925.
- Dee, D., et al. (2011), The ERA-Interim reanalysis: Configuration and performance of the data assimilation system, *Quarterly Journal of the Royal Meteorological Society*, *137*(656), 553–597.
- Desjardins, R., J. MacPherson, P. Schuepp, and F. Karanja (1989), An evaluation of aircraft flux measurements of CO₂, water vapor and sensible heat, in *Boundary Layer Studies and Applications*, pp. 55–69, Springer.
- 20 Elberling, B., and K. K. Brandt (2003), Uncoupling of microbial CO₂ production and release in frozen soil and its implications for field studies of arctic C cycling, *Soil Biology and Biochemistry*, *35*(2), 263–272.
- Esau, I., and I. Repina (2012), Wind climate in Kongsfjorden, Svalbard, and attribution of leading wind driving mechanisms through turbulence-resolving simulations, *Advances in Meteorology*, 2012.
- Fahnestock, J. T., M. H. Jones, and J. M. Welker (1999), Wintertime CO₂ efflux from arctic soils: implications for annual carbon budgets,
25 *Global Biogeochemical Cycles*, *13*(3), 775–779.
- Falge, E., et al. (2001), Gap filling strategies for defensible annual sums of net ecosystem exchange, *Agricultural and forest meteorology*, *107*(1), 43–69.
- Foken, T., and B. Wichura (1996), Tools for quality assessment of surface-based flux measurements, *Agricultural and forest meteorology*, *78*(1), 83–105.
- 30 Foken, T., F. Wimmer, M. Mauder, C. Thomas, and C. Liebethal (2006), Some aspects of the energy balance closure problem, *Atmospheric Chemistry and Physics*, *6*(12), 4395–4402.
- Førland, E. J., R. Benestad, I. Hanssen-Bauer, J. E. Haugen, and T. E. Skaugen (2012), Temperature and precipitation development at Svalbard 1900–2100, *Advances in Meteorology*, 2011.
- Fortier, D., M. Allard, and Y. Shur (2007), Observation of rapid drainage system development by thermal erosion of ice wedges on Bylot
35 Island, Canadian Arctic Archipelago, *Permafrost and Periglacial Processes*, *18*(3), 229–243.
- Fratini, G., and M. Mauder (2014), Towards a consistent eddy-covariance processing: an intercomparison of EddyPro and TK3, *Atmospheric Measurement Techniques*, *7*(7), 2273–2281.



- Grosse, G., V. Romanovsky, T. Jorgenson, K. W. Anthony, J. Brown, and P. P. Overduin (2011), Vulnerability and feedbacks of permafrost to climate change, *Eos, Transactions American Geophysical Union*, 92(9), 73–74.
- Harris, C., et al. (2009), Permafrost and climate in Europe: Monitoring and modelling thermal, geomorphological and geotechnical responses, *Earth-Science Reviews*, 92(3), 117–171.
- 5 Johansson, M., T. V. Callaghan, J. Bosio, H. J. Åkerman, M. Jackowicz-Korczynski, and T. R. Christensen (2013), Rapid responses of permafrost and vegetation to experimentally increased snow cover in sub-arctic Sweden, *Environmental Research Letters*, 8(3), 035,025.
- Jorgenson, M. T., Y. L. Shur, and E. R. Pullman (2006), Abrupt increase in permafrost degradation in Arctic Alaska, *Geophysical Research Letters*, 33(2).
- Jorgenson, M. T., M. Kanevskiy, Y. Shur, N. Moskalenko, D. Brown, K. Wickland, R. Striegl, and J. Koch (2015), Role of ground ice
10 dynamics and ecological feedbacks in recent ice wedge degradation and stabilization, *Journal of Geophysical Research: Earth Surface*, 120(11), 2280–2297.
- Kljun, N., P. Calanca, M. Rotach, and H. Schmid (2015), A simple two-dimensional parameterisation for Flux Footprint Prediction (FFP), *Geoscientific Model Development*, 8(11), 3695–3713.
- Kutzbach, L., C. Wille, and E.-M. Pfeiffer (2007), The exchange of carbon dioxide between wet arctic tundra and the atmosphere at the Lena
15 River Delta, Northern Siberia, *Biogeosciences*, 4(5), 869–890.
- Lee, X., W. Massman, and B. Law (2006), *Handbook of micrometeorology: a guide for surface flux measurement and analysis*, vol. 29, Springer Science & Business Media.
- Leffingwell, E. d. K. (1915), Ground-ice wedges: The dominant form of ground-ice on the north coast of Alaska, *The Journal of Geology*, 23(7), 635–654.
- 20 Liljedahl, A. K., et al. (2016), Pan-Arctic ice-wedge degradation in warming permafrost and its influence on tundra hydrology, *Nature Geoscience*.
- Lucieer, A., S. de Jong, and D. Turner (2013), Mapping landslide displacements using Structure from Motion (SfM) and image correlation of multi-temporal UAV photography, *Progress in Physical Geography*, p. 0309133313515293.
- Lüers, J., S. Westermann, K. Piel, and J. Boike (2014), Annual CO₂ budget and seasonal CO₂ exchange signals at a High Arctic permafrost
25 site on Spitsbergen, Svalbard archipelago, *Biogeosciences*, 11(22), 6307–6322.
- Lund, M., J. M. Falk, T. Friborg, H. N. Mbufong, C. Sigsgaard, H. Soegaard, and M. P. Tamstorf (2012), Trends in CO₂ exchange in a high Arctic tundra heath, 2000–2010, *Journal of Geophysical Research: Biogeosciences*, 117(G2).
- Mackay, J. R. (1974), Ice-wedge cracks, Garry Island, Northwest Territories, *Canadian Journal of Earth Sciences*, 11(10), 1366–1383.
- Mbufong, H., et al. (2014), Assessing the spatial variability in peak season CO₂ exchange characteristics across the Arctic tundra using a
30 light response curve parameterization, *Biogeosciences*, 11(17), 4897–4912.
- McGuire, A., et al. (2012), An assessment of the carbon balance of Arctic tundra: comparisons among observations, process models, and atmospheric inversions, *Biogeosciences*, 9(8), 3185–3204.
- Minke, M., N. Donner, N. S. Karpov, P. de Klerk, and H. Joosten (2007), Distribution, diversity, development and dynamics of polygon mires: examples from Northeast Yakutia (Siberia), *Peatlands International*, 1, 36–40.
- 35 Moncrieff, J., R. Clement, J. Finnigan, and T. Meyers (2004), Averaging, detrending, and filtering of eddy covariance time series, in *Handbook of micrometeorology*, pp. 7–31, Springer.
- Moncrieff, J. B., et al. (1997), A system to measure surface fluxes of momentum, sensible heat, water vapour and carbon dioxide, *Journal of Hydrology*, 188, 589–611.



- Natali, S. M., E. A. Schuur, C. Trucco, C. E. HICKS PRIES, K. G. Crummer, and A. F. BARON LOPEZ (2011), Effects of experimental warming of air, soil and permafrost on carbon balance in Alaskan tundra, *Global Change Biology*, 17(3), 1394–1407.
- Necsoiu, M., C. L. Dinwiddie, G. R. Walter, A. Larsen, and S. A. Stothoff (2013), Multi-temporal image analysis of historical aerial photographs and recent satellite imagery reveals evolution of water body surface area and polygonal terrain morphology in Kobuk Valley National Park, Alaska, *Environmental Research Letters*, 8(2), 025,007.
- 5 Nordli, Ø., R. Przybylak, A. E. Ogilvie, and K. Isaksen (2014), Long-term temperature trends and variability on Spitsbergen: the extended Svalbard Airport temperature series, 1898–2012, *Polar research*, 33.
- Oechel, W. C., C. A. Laskowski, G. Burba, B. Gioli, and A. A. Kalhori (2014), Annual patterns and budget of CO₂ flux in an Arctic tussock tundra ecosystem, *Journal of Geophysical Research: Biogeosciences*, 119(3), 323–339.
- 10 Osterkamp, T., M. Jorgenson, E. Schuur, Y. Shur, M. Kanevskiy, J. Vogel, and V. Tumskoy (2009), Physical and ecological changes associated with warming permafrost and thermokarst in interior Alaska, *Permafrost and Periglacial Processes*, 20(3), 235–256.
- Pirk, N., M. P. Tamstorf, M. Lund, M. Mastepanov, S. H. Pedersen, M. R. Mylius, F.-J. W. Parmentier, H. H. Christiansen, and T. R. Christensen (2016a), Snowpack fluxes of methane and carbon dioxide from high Arctic tundra, *Journal of Geophysical Research: Biogeosciences*, 121, 1–15, doi:10.1002/2016JG003486.
- 15 Pirk, N., M. Mastepanov, F.-J. W. Parmentier, M. Lund, P. Crill, and T. R. Christensen (2016b), Calculations of automatic chamber flux measurements of methane and carbon dioxide using short time series of concentrations, *Biogeosciences*, 13(4), 903–912.
- Reichstein, M., et al. (2005), On the separation of net ecosystem exchange into assimilation and ecosystem respiration: review and improved algorithm, *Global Change Biology*, 11(9), 1424–1439.
- Romanovskii, N. (1985), Distribution of recently active ice and soil wedges in the USSR, *Field and theory*, pp. 154–165.
- 20 Romanovsky, V. E., S. L. Smith, and H. H. Christiansen (2010), Permafrost thermal state in the polar northern hemisphere during the international polar year 2007–2009: a synthesis, *Permafrost and Periglacial Processes*, 21(2), 106–116.
- Schuur, E., et al. (2015), Climate change and the permafrost carbon feedback, *Nature*, 520(7546), 171–179.
- Seok, B., D. Helmig, M. W. Williams, D. Liptzin, K. Chowanski, and J. Hueber (2009), An automated system for continuous measurements of trace gas fluxes through snow: an evaluation of the gas diffusion method at a subalpine forest site, Niwot Ridge, Colorado,
- 25 *Biogeochemistry*, 95(1), 95–113.
- Sievers, J., L. L. Sørensen, T. Papakyriakou, B. Else, M. Sejr, D. Haubjerg Søgaard, D. Barber, and S. Rysgaard (2015a), Winter observations of CO₂ exchange between sea ice and the atmosphere in a coastal fjord environment, *The Cryosphere*, 9(4), 1701–1713.
- Sievers, J., T. Papakyriakou, S. E. Larsen, M. M. Jammet, S. Rysgaard, M. K. Sejr, and L. Sørensen (2015b), Estimating surface fluxes using eddy covariance and numerical ogive optimization, *Atmospheric Chemistry and Physics*, 15(4), 2081–2103, toolbox publicly available through the Mathworks file exchange: <http://se.mathworks.com/matlabcentral/fileexchange/53545-ogive-optimization-toolbox>.
- 30 Smagin, A., and N. Shnyrev (2015), Methane fluxes during the cold season: distribution and mass transfer in the snow cover of bogs, *Eurasian Soil Science*, 48(8), 823–830.
- Snavely, N., S. M. Seitz, and R. Szeliski (2008), Skeletal graphs for efficient structure from motion, in *CVPR*, vol. 1, p. 2.
- Soegaard, H., and C. Nordstroem (1999), Carbon dioxide exchange in a high-arctic fen estimated by eddy covariance measurements and modelling, *Global Change Biology*, 5(5), 547–562.
- Takagi, K., M. Nomura, D. Ashiya, H. Takahashi, K. Sasa, Y. Fujinuma, H. Shibata, Y. Akibayashi, and T. Koike (2005), Dynamic carbon dioxide exchange through snowpack by wind-driven mass transfer in a conifer-broadleaf mixed forest in northernmost Japan, *Global Biogeochemical Cycles*, 19(2).



- Ullman, S. (1979), The interpretation of structure from motion, *Proceedings of the Royal Society of London B: Biological Sciences*, 203(1153), 405–426.
- Vaughn, L. J., M. E. Conrad, M. Bill, and M. S. Torn (2016), Isotopic insights into methane production, oxidation, and emissions in arctic polygon tundra, *Global Change Biology*.
- 5 Vickers, D., and L. Mahrt (1997), Quality control and flux sampling problems for tower and aircraft data, *Journal of Atmospheric and Oceanic Technology*, 14(3), 512–526.
- Wegener, C., and A. M. Odasz-Albrigtsen (1998), Do Svalbard reindeer regulate standing crop in the absence of predators?, *Oecologia*, 116(1-2), 202–206.
- Westoby, M., J. Brasington, N. Glasser, M. Hambrey, and J. Reynolds (2012), ‘Structure-from-Motion’ photogrammetry: A low-cost, effective
10 tool for geoscience applications, *Geomorphology*, 179, 300–314.